Atmospheric factors outweigh species traits and soil properties in explaining spatiotemporal variation in water-use efficiency of tropical and subtropical forest species

Songbo Tang [a,b,c], Hilary Rose Dawson [d], Lucas C.R. Silva [d], Josep Peñuelas [e,f], Jordi Sardans [e,f], Hans Lambers [g,h], Feiyan Zeng [i], Yuan Lai [a,b,c], Yanlong Jia [j], Guoyi Zhou [k], Yunting Fang [l], Ying Tu [l], Dan Xi [m], Dianxiang Zhang [i,*], Yuanwen Kuang [a,b,*]

[a] Key Laboratory of Vegetation Restoration and Management of Degraded Ecosystems, South China Botanical Garden, Chinese Academy of Sciences, Guangzhou 510650, China
[b] Guangdong Provincial Key Laboratory of Applied Botany, Guangzhou 510650, China
[c] College of Resources and Environment, University of Chinese Academy of Sciences, Beijing 100049, China
[d] Department of Biology. University of Oregon. Institute of Ecology and Evolution. Eugene, OR 97403, United States
[e] CSIC, Global Ecology Unit, CREAF-CSIC-UAB, Bellaterra, 08193 Barcelona, Catalonia, Spain
[f] CREAF, Cerdanyola del Vallès 08193, Catalonia, Spain
[g] School of Biological Sciences, University of Western Australia, Perth, WA 6009, Australia
[h] Department of Plant Nutrition, College of Resources and Environmental Sciences; National Academy of Agriculture Green Development; Key Laboratory of Plant–Soil Interactions, Ministry of Education; China Agricultural University, Beijing 100193, China
[i] Key Laboratory of Plant Resources Conservation and Sustainable Utilization, South China Botanical Garden, Chinese Academy of Sciences, Guangzhou 510650, China
[j] Key Laboratory of Ecosystem Network Observation and Modeling, Institute of Geographic Sciences and Natural Resources Research, Chinese Academy of Sciences, Beijing 100101, China
[k] Institute of Ecology, Nanjing University of Information Science and Technology, Nanjing 210044, China
[l] Key Laboratory of Forest Ecology and Management, Institute of Applied Ecology, Chinese Academy of Sciences, Shenyang 110016, China
[m] Lushan Botanical Garden, Chinese Academy of Sciences, Jiujiang 332900, China

ARTICLE INFO

ABSTRACT

Intrinsic water-use efficiency (iWUE) is a key physiological trait; however, the spatiotemporal variation in iWUE and which factors affect iWUE in the tropics and subtropics are poorly known. We determined the temporal (1920-2010) and spatial patterns of iWUE using leaf carbon-isotopic composition (δ^{13}C) of 1,811 herbarium specimens and associated these patterns with environmental factors across biomes in southern China. We found that iWUE increased by 15.7 µmol mol^{-1} in the entire studied area from 1920 to 2010. The iWUE declined from west to east in southern China, with higher values concentrated in the southwest. Rising CO_2 concentrations ([CO_2]), N deposition, increases in mean annual temperature (MAT) and vapor pressure deficit (VPD), and changes in temperature seasonality (TS) contributed to the spatiotemporal changes in iWUE. Our results confirm that, in addition to a continuous increase in iWUE has, the rate of change of iWUE decreased in southern China in the later years. Multiple atmospheric factors jointly determine the changes in both iWUE and the rate of change of iWUE in the studied regions.

1. Introduction

Over the past century, the physiology of plants has changed in response to rising atmospheric carbon dioxide concentrations ([CO_2]), global warming, changes in precipitation, and increased nitrogen (N) deposition (Adams et al., 2020; Soh et al., 2019). This change can be observed in leaf functional traits from stomatal to organ levels (Soh et al., 2019) and has altered carbon-water relationships from individual plants to forest ecosystems (Cernusak et al., 2019; Maxwell et al., 2018; Vogado et al., 2020).

By definition, water-use efficiency (WUE) is closely associated with carbon fixation and water loss in plants (Cernusak et al., 2019), and with

net primary production of ecosystems by altering carbon-water cycles (Adams et al., 2020). Foliar carbon-isotopic composition (expressed as $\delta^{13}C$) is widely used as a proxy for intrinsic WUE (iWUE) (Farquhar et al., 1982; Huang et al., 2016; Peñuelas et al., 2011). Based on the $\delta^{13}C$ of tree rings or specimens, for example, previous studies showed that plant iWUE increased over the past decades globally or regionally (Huang et al., 2016; McLauchlan et al., 2010; Peñuelas et al., 2011) which can be affected by biotic and abiotic factors such as species (Soh et al., 2019), vapor pressure deficit (VPD), temperature, wind speed, and soil properties (Cornwell et al., 2018; Maxwell et al., 2018). On the other hand, there some different views about the correlations between plant iWUE and environmental changes. Specifically, a growing number of studies suggest that we have overestimated the effect of CO_2 on plant iWUE, and that the effect of CO_2 on iWUE is diminishing at a global scale (Adams et al., 2020; Marchand et al., 2020).

Tropical and subtropical forests in southern China represent the largest terrestrial sink for CO_2 in China (Wang et al., 2020a) and have been affected by many facets of global change, e.g., atmospheric CO_2 and N deposition, over the past hundred years (Liu et al., 2013; Yu et al., 2019). It is well established that abiotic factors, e.g., atmospheric $[CO_2]$, soil, and climate and their interactions affect iWUE (Giguere-Croteau et al., 2019; Quadri et al., 2021; Silva et al., 2016). However, the changes in iWUE and their driving factors in the long term and at large scales are poorly studied in southern China's forests in comparison with well-studied ecosystems in other biomes in central and north China, e.g., temperate deciduous and montane coniferous forests (Liu et al., 2018). This is because of the many challenges accessing reliable field sites in that remote region where there are a limited number of research institutes to provide adequate data and materials for this type of study. Understanding how iWUE in tropical and subtropical ecosystems temporally and spatially responds and which factors drive the responses that may differ from findings from temperate biomes (Huang et al., 2017), is important for assessing the forest structure and functioning to global change.

Temporal changes in iWUE can be quantified via $\delta^{13}C$ values in tree ring series (Adams et al., 2020). Previous studies have shown small variation in $\delta^{13}C$ values (typically $< 1‰$) between co-located old and young trees within systems as diverse as tropical montane forests of Mexico (Quadri et al., 2021) and alpine tree lines of Tibet (Silva et al., 2016). However, the annually-resolved "replication" of $\delta^{13}C$ values among adjacent tree rings can sometimes not be considered as independent measures indicating the temporal shifts in iWUE in response to changes in climate and CO_2 concentration. To address this limitation, we used independent records from multiple plant species collected across broad environmental gradients, using a hierarchical spatial design as proposed by Maxwell et al. (2018), combined with historical data of leaves from independently collected herbarium specimens of the same species. We tested these hypotheses: 1) iWUE generally increased in response to rising atmospheric $[CO_2]$, but the strength of that response varied predictably across regions depending on climatic conditions (e.g., subtropical and tropical forests of China show different sensitivities in that response) reflecting patterns observed in other parts of the world (Adams et al., 2020; McLauchlan et al., 2010; Peñuelas et al., 2011). 2) Within biomes, iWUE varied among species (e.g., due to species traits) and site conditions (e.g., due to soil properties) (Maxwell et al., 2018). Testing these hypotheses will improve our ability to develop theoretical and computational scenarios to predict changes in the carbon-water cycle of forest ecosystems under global change.

2. Materials and Methods

2.1. Specimen collection

We selected 12 common broad-leaved species (five shrub and seven tree species, Table S1) for foliar collection based on their wide distribution in tropical and subtropical forests of China (18–34°N, 97–122°E).

All were sampled from the Herbarium of South China Botanical Garden, Chinese Academy of Science (IBSC, http://herbarium.scbg.cas.cn/). We collected at least three leaves from each preserved herbarium sheet that met the criteria of 1) complete spatial and temporal metadata, 2) free from chemical treatments that might influence the analysis, and 3) conspicuous flowers and/or fruits on herbarium specimens. Although herbarium labels did not indicate the canopy position that the leaves were sampled from, leaves of shrubs and herbs generally were collected from the understory, while leaves of trees were collected from the sun-exposed side of the canopy. During the processes of collecting leaves from herbarium specimens, we sampled lower down on each branch to obtain leaves that were as mature as possible to decrease the effects of young leaves on $\delta^{13}C$ values (Vogado et al., 2020). We collected leaves from a total of 1,811 out of 5,835 possible herbarium specimens, spanning 90 years (1920–2010) and located at 429 sites in subtropical and tropical forests of southern China (Fig. S1, S2; Table S2).

2.2. Leaf variables

All analyses were performed in R v 4.0.3 (R Core Team, 2020), except where otherwise indicated. In the following methods, we denote functions used with the format of package::function to improve analysis replicability.

We carefully cut off the leaves from each specimen and kept them in a sealed bag. We dried the samples to a constant weight at 65°C for 72 hours and ground them before analysis. We determined C and N concentrations and stable C isotopes with a mass spectrometer (Thermo Finnigan, North Pod Waltham, Massachusetts, USA) coupled with an elemental analyzer (Costech Analytical Technologies, Valencia, California, USA).

We calculated iWUE based on the $\delta^{13}C$ values according to Farquhar and Richards (1984) and Ehleringer and Cerling (1995). We discarded 395 of the initial 1,811 measurements, because they were outside the expected $\delta^{13}C$ values range of -30 to -22‰ (Cerling et al., 1997) or outside our four climatic regions. We calculated stomatal isotopic fractionation using the measured values for each plant sample ($\delta^{13}C_p$) and annual $\delta^{13}C$ values of the air ($\delta^{13}C_a$) derived from Graven et al. (2017) (Eq. (1)), and adjusted for elevation and the Suess effect using a modified version of the pin function of McCarroll et al. (2009). We calculated C isotopic discrimination ($\Delta^{13}C$) via Eq. (1):

$$\Delta^{13}C = \left(\delta^{13}C_a - \delta^{13}C_p\right) \Big/ \left(1 + \frac{\delta^{13}C_p}{1,000}\right) \qquad (1)$$

We calculated the ratios of internal CO_2 (C_i) to atmospheric CO_2 concentration (C_a, data are from NASA GISS [https://data.giss.nasa.gov/modelforce/ghgases/]), using Eq. (2):

$$\frac{C_i}{C_a} = \left(\Delta^{13}C + f\frac{\Gamma_*}{C_a} - a_s\right) \Big/ (b - a_s) \qquad (2)$$

where a_s and b indicate the stomatal diffusive and photosynthetic fractionation constants, respectively (a_s: 4.4‰ and b: 27‰) (Farquhar and Richards, 1984); f is the fractionation associated with photorespiration ($\approx 12‰$) (Lanigan et al., 2008; Marchand et al., 2020); r^* is the CO_2 compensation point in the absence of mitochondrial respiration, representing the temperature of the photosynthetically active period (Bernacchi et al., 2001), which is obtained by mean annual temperature and elevation via Eq. (3) using the rpmodel::gammastar function (Bernacchi et al., 2001; Stocker et al., 2020).

$$\Gamma_* = 4.332 \times \frac{P_{atm}}{101.3} \times \exp\left(378.3 \times \frac{MAT - 25}{298.15 \times 8.3145 \times (MAT + 273.15)}\right) \qquad (3)$$

where MAT is mean annual temperature; P_{atm} (Pa) is atmospheric pressure, obtained from site elevation via Eq. (4) using the rpmodel::
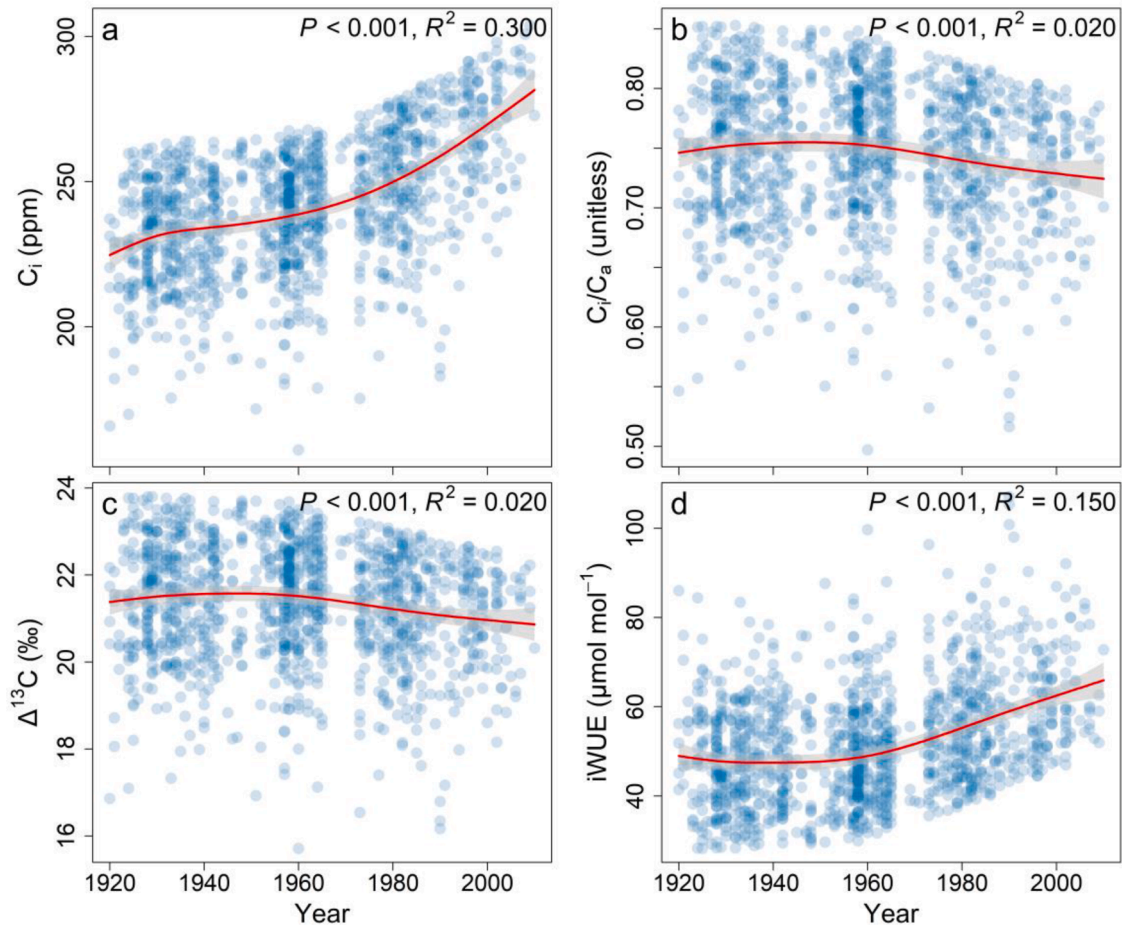
Fig. 1. Temporal patterns of the intracellular CO_2 concentration (a, C_i), the ratio of intracellular CO_2 concentration to atmospheric CO_2 concentration (b, C_i/C_a), $\Delta^{13}C$ (c), and iWUE (d) in southern China over the past 90 years. Blue dots represent partial residuals from the generalized additive mixed models (GAMMs), that is, the estimates for the variable plus the residuals. Red lines and gray shadings are, respectively, for the predicted values and 95% confidence intervals from the GAMMs.

patm function (Allan et al., 1998; Stocker et al., 2020).

$$P_{atm} = 101325 \times \left(\frac{298.15 - 0.0065 \times z}{298.15} \right)^{5.26} \tag{4}$$

where z is the elevation above sea level (m).

We then solved this for iWUE, using the ratio of water vapor to CO_2 diffusivity (1.6) via Eq. (5) (Huang et al., 2016):

$$iWUE = \frac{A}{g_s} = \frac{1 - \frac{C_i}{C_a}}{\frac{1.6}{C_a}} \tag{5}$$

2.3. Environmental factors

We used partial pressure of CO_2 (P_{CO_2}, Eq. (6)) to test the correlations between iWUE and [CO_2] (Marchand et al., 2020).

$$P_{CO_2} = 10^{-6} \times CO_2 \times P_{atm} \tag{6}$$

where P_{atm} is atmospheric pressure, obtained from Eq. (4).

We extracted monthly mean temperature, mean vapor pressure (VAP), and mean potential evapotranspiration (PET), total precipitation, maximum and minimum temperature (T_{max} and T_{min}, respectively) from Climate Research Unit (CRU) TS v4.05 (Harris et al., 2020), and extracted monthly wind speed and solar radiation during 1920-2010 from the Terrestrial Hydrology Research Group at Princeton University (Sheffield et al., 2006). The spatial and temporal resolution of the above datasets are 0.5° and month, respectively. We calculated mean

annual temperature (MAT), mean annual precipitation (MAP), temperature and precipitation seasonality (TS and PS, respectively) with dismo::biovars based on monthly precipitation, T_{max} and T_{min} (Fick and Hijmans, 2017), and calculated vapor pressure deficit (VPD) based on VAP and monthly temperature (Grossiord et al., 2020). We defined leaf C/N ratio (tested in this study), CO_2, MAT, MAP, TS, PS, VPD, PET, wind speed, and solar radiation as time series factors because there are annual values for these factors from 1920 to 2010.

We extracted pH values, cation-exchange capacity (CEC), clay (Clay) and silt (Silt) content, soil organic matter (SOM), available nitrogen (AN) and phosphorus (AP) concentration, and total nitrogen (TN) and phosphorus (TP) concentration at 0-80 cm depth in soil in forests across China from Shangguan et al. (2013). Total mean N deposition (Ndep) during 1990-2010 at each site was extracted from Jia et al. (2019). The spatial resolution of the above datasets is 30 arc-seconds. We defined soil pH, CEC, Clay, Silt, SOM, TN, TP, AN, AP, and N deposition at our sites as non-time series factors.

2.4. Statistical analyses

We averaged foliar C_i, C_i/C_a ratios, $\Delta^{13}C$ values and iWUE of same species at the same site (defined as all specimens within each 0.1° latitude and longitude) within a year. Therefore, we had 1,286 observations included in data analyses.

We performed variance partition of foliar C_i, C_i/C_a ratios, $\Delta^{13}C$ values and iWUE to determine the relative effect of time, space (latitude and longitude), and species over the past 90 years via the vegan::varpart
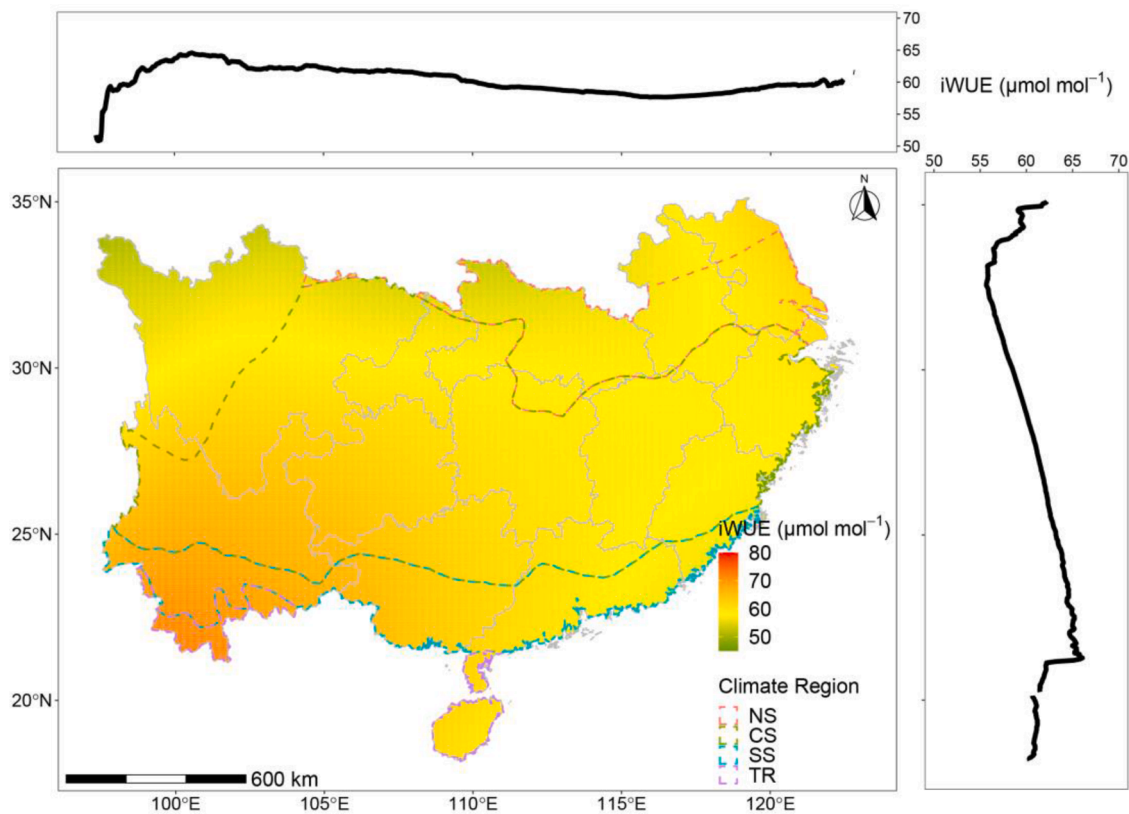
Fig. 2. Spatial pattern of intrinsic water-use efficiency (iWUE, n =152, the sites where samples were collected) over the period of 1990-2010. Black lines in top and right panel indicate the variation of iWUE along longitude and latitude. NS: northern subtropics, CS: central subtropics, SS: southern subtropics; and TR: tropics. The spatial pattern of iWUE was obtained by Kriging interpolation in ArcGIS 10.3 for Desktop.

function (Peres-Neto et al., 2006). We used Mann-Kendall trend test via the trend::mk.test function to test the trend of iWUE over the past 90 years. We calculated the annual rate of change in iWUE (defined as mean changed value in iWUE each year) with a 45-year moving window for each species from 1920 to 2010 (Wang et al., 2020b). Specifically, we set 45 years as sliding windows (e.g., 1920-1965, 1921-1966, …,1965-2010) to capture long-term responses in a temporally replicated manner, rather than high-frequency variation in ecophysiological performance, which may arise, for example, from single extreme weather events. Accordingly, the regression slopes of sampling year and plant performance were generated for each window using the annually-resolved rate of change calculated for iWUE. We used a 45-year moving window, because the sample size of each species in each year was too small to fit by linear regression; 45 years was the largest window, and this window avoided data overlap between the first- and last-time window.

We determined the effects of environmental factors on temporal and spatial patterns of iWUE in two steps. First, we tested the correlation between multiple environmental factors and plant iWUE based on our datasets; and, second, we assessed how these factors affected the temporal and spatial patterns of plant iWUE based on the temporal and spatial variation of each important factor. We used all data (n = 1,416) to tested the correlations between time-series factors and plant iWUE. Meanwhile, we subdivided our data from 1990 to 2010 (n = 152) to test the correlations between iWUE and non-time-series factors in southern China, since there is no available high-quality and long-term dataset of soil factors and N deposition (i.e. soil properties and N deposition). There are three reasons why we selected samples during 1990-2010: 1) the narrow time span can decline the effects of sampling year on the analyses related with no-time serial factors; 2) the soil properties extracted from Shangguan et al. (2013) were derived using soil profiles sampled in the Second National Soil Survey during 1979–1985; and 3)

the temporal variation for soil properties was small compared with spatial variation (Poggio et al., 2021). We divided the sampling sites for the historical specimens into four ecological regions, namely northern subtropical region (NS), central subtropical region (CS), southern subtropical region (SS), and tropical region (TR), based on Chinese vegetation regionalization (http://www.resdc.cn/data.aspx?DATAID =125), and into four soil types based on criteria of the United States Department of Agriculture (Hengl et al., 2017), namely Alfisols, Entisols, Inceptisols, and Ultisols. We tested the difference in iWUE via linear mixed effect models along ecological regions and soil types, with year and species as random effects (Crawley, 2012). We determined differences in iWUE among ecological regions and soil types with Tukey's honestly significant difference (HSD) post–hoc test with lsmeans::lsmeans (Lenth, 2016).

There are two steps to determine the correlations of multiple environmental factors on iWUE. First, we calculated the relative importance of all environmental factors as described by Du et al. (2020) and Terrer et al. (2016). In brief, we calculated a series of models and extracted Akaike weight of all possible models using the glmulti:: glmulti function (Calcagno and de Mazancourt, 2010), and then calculated the relative importance of factors by summing the Akaike weights for the models in which the environmental factor was included (Calcagno and de Mazancourt, 2010; Terrer et al., 2016). A critical relative importance value of 0.8 was set to distinguish between the important and less important environmental factors (Du et al., 2020; Terrer et al., 2016). Second, after obtaining these important factors, we used generalized additive mixed models (GAMM) to examine the relationship between iWUE and environmental factors with high relative importance (> 0.8) with the formula: iWUE~1+s(factor 1)+s(factor 2)+…+s(factor n)+ $(\frac{\text{site}}{\text{Species}})$ + corCAR1(year$|\frac{\text{site}}{\text{Species}}$). In this formula, factors 1, 2, …, and n indicate the environmental factors with relative importance over 0.8,
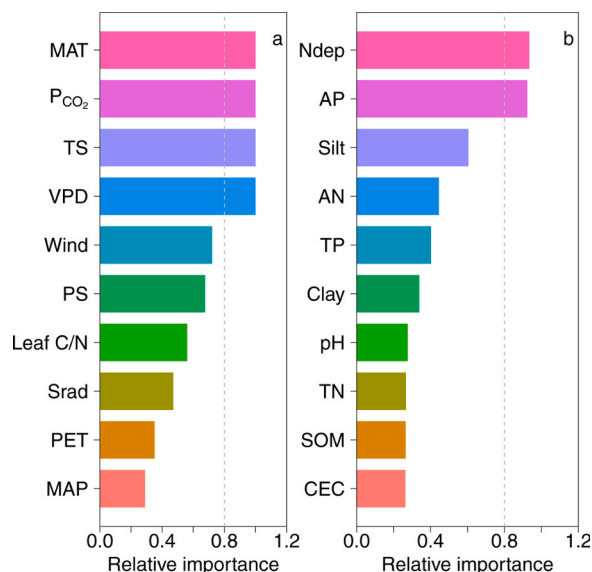
Fig. 3. Relative importance of time series (a, 1920-2010) and non-time series (b, 1990-2010) environmental factors on leaf iWUE. Relative importance derived from the sum of the Akaike weights based on the results of model selection using Akaike information criterion (AIC). Gray dashed lines indicate cutoff values of relative importance (0.8) which distinguished important and unimportant. MAT: mean annual temperature; P_{CO_2}: partial pressure of atmospheric CO_2; TS: temperature seasonality; VPD: vapor pressure deficit; Wind: wind speed; PS: precipitation seasonality; leaf C/N: the ratio of leaf carbon to nitrogen concentrations; Srad: solar radiation; PET: potential evapotranspiration; MAP: mean annual precipitation; Ndep: total N deposition; AP: available phosphorus concentration; Silt: soil silt content; AN: available nitrogen concentration; TP: soil total phosphorus concentration; Clay: soil clay content; pH: soil pH; CEC: soil cation exchange capacity; TN: soil total nitrogen concentration; and SOM: soil organic matter.

Table 1

Summaries of generalized additive mixed models (GAMMs). EDF: Estimated degree of freedom; IR^2: incremental R^2; P_{CO_2}: partial pressure of CO_2, VPD: vapor pressure deficit, MAT: mean annual temperature, TS: temperature seasonality (TS).

	Factor	EDF	F	IR^2	P	R^2
Time series (1920-2010)	P_{CO_2}	3.73	46.65	0.09	< 0.001	0.21
	VPD	2.37	8.60	0.02	< 0.001	
	MAT	1.00	128.8	0.07	< 0.001	
	TS	3.94	14.88	0.03	< 0.001	
Non-time series (1990-2010)	N deposition	1.00	9.97	0.06	0.002	0.06
	Available P	1.00	1.32		< 0.01	0.253

$\frac{site}{Species}$ represents the random effect of species nested within sample site, and corCAR1 allows for unequally spaced observations (Marchand et al., 2020). We used the vegan::varpart function to calculate the variance partition of each environmental factor that was significantly correlated with iWUE in GAMMs on iWUE (Peres-Neto et al., 2006). We established two full GAMMs (Table S3) based on all environmental factors focused on this study to test if there was omission of environmental factors from the results of the first step. The results showed that all the significant factors in GAMMs had a high relative importance in the first step.

We performed dominance analysis to calculate the incremental R^2 (IR^2) of important factors to plant iWUE (Azen and Budescu, 2003; Zhao et al., 2022). Single-factor in the full GAMM was picked and fitted into

the GAMM to develop a series of sub-models (Zhao et al., 2022). The IR^2 of each environmental factor was derived via averaging all the differences between each possible sub-model excluding or including the relevant factor. Significance was set at $P < 0.05$.

3. Results

3.1. Spatiotemporal patterns of iWUE

Foliar C_i, C_i/C_a ratios, $\Delta^{13}C$ values and iWUE varied with time (year) and space (longitude and/or latitude, Fig. S3) which supports a part of hypothesis one. Overall, foliar $\Delta^{13}C$ values and C_i/C_a decreased, but foliar C_i and iWUE increased by 46 ppm and 15.7 µmol mol^{-1}, respectively (Fig. 1, Table S4). Consistent patterns of change in C_i, C_i/C_a, $\Delta^{13}C$, and iWUE (Table S5) were observed in all studied species (Fig. S4), life forms (Fig. S5), leaf types (Fig. S5), ecological regions (Fig. S6), and soil types (Fig. S7). However, the moving window of iWUE showed a nonlinear change, with slow, fast, and constant rates at the first, middle, and late periods of 1920-2010, respectively (Fig. S8). Intrinsic water-use efficiency did not vary spatially among the four regions and soil types (Fig. S9). However, iWUE was higher in the southwest than in other regions in our study (Fig. 2).

3.2. Correlations between factors and iWUE

For climatic and biotic factors, the relative importance of four factors, i.e. P_{CO_2}, VPD, MAT, and TS, were over 0.8 (Fig. 3a). All these relatively important factors significantly affected iWUE (Table 1), with P_{CO_2} and VPD positively, but MAT and TS negatively affecting iWUE (Fig. 4). The four factors explained 21% of the variation of plant iWUE of all samples collected during 1920-2010 (Table 1). Two non-time series factors, i.e. N deposition and available phosphorus had a high relative impact on iWUE (Fig. 3b, Table 1), but only N deposition was significantly correlated with plant iWUE (Fig. 4). Nitrogen and available phosphorus explained 7% of the variations of iWUE of samples collected during 1990-2010 (Table 1). The P_{CO_2}, N deposition, MAT, TS, and VPD explained approximately 9, 7, 7, 3, and 2% of the total variation of iWUE in southern China's forests (Table 1).

4. Discussion

The present results indicate that there was a huge temporal and spatial variability in iWUE in southern China's forests over the past nine decades, and the variabilities of iWUE were not only associated with atmospheric CO_2 concentrations, but also greatly affected by climatic, i.e. MAT, TS, VPD, and N deposition in southern China over the past 90 years, confirming that multiple environmental factors affect plant iWUE (Cornwell et al., 2018; Maxwell et al., 2018; Silva and Lambers, 2021; Tang et al., 2022). Nevertheless, the increased patterns of plant iWUE were observed for all species, ecological regions, and soil types. The uniform patterns might be related to the important role of atmospheric CO_2 in impacting carbon-water exchange in plants (Peñuelas et al., 2011), which is consistent with a part of our first hypothesis that iWUE has generally increased in response to rising atmospheric [CO_2]. The significant increase of iWUE in forests of southern China over the past 90 years is consistent with the patterns found by McLauchlan et al. (2010) using specimens spanning 130 years in temperate grasslands, and by Peñuelas et al. (2011) using a global database covering all major forest biome types, but inconsistent with Huang et al. (2016), who found that iWUE decreased by 30% from the 1950s to 2010.

The overall temporal patterns of increasing iWUE in this study and others, e.g., Peñuelas et al. (2011) and McLauchlan et al. (2010), might be caused by decreases in stomatal conductance due to elevated atmospheric [CO_2]. Additionally, the changes in VPD, N deposition, and TS also contributed to the temporal patterns of iWUE over the past 90 years in southern China (Fig. S10). It is generally well understood that a high
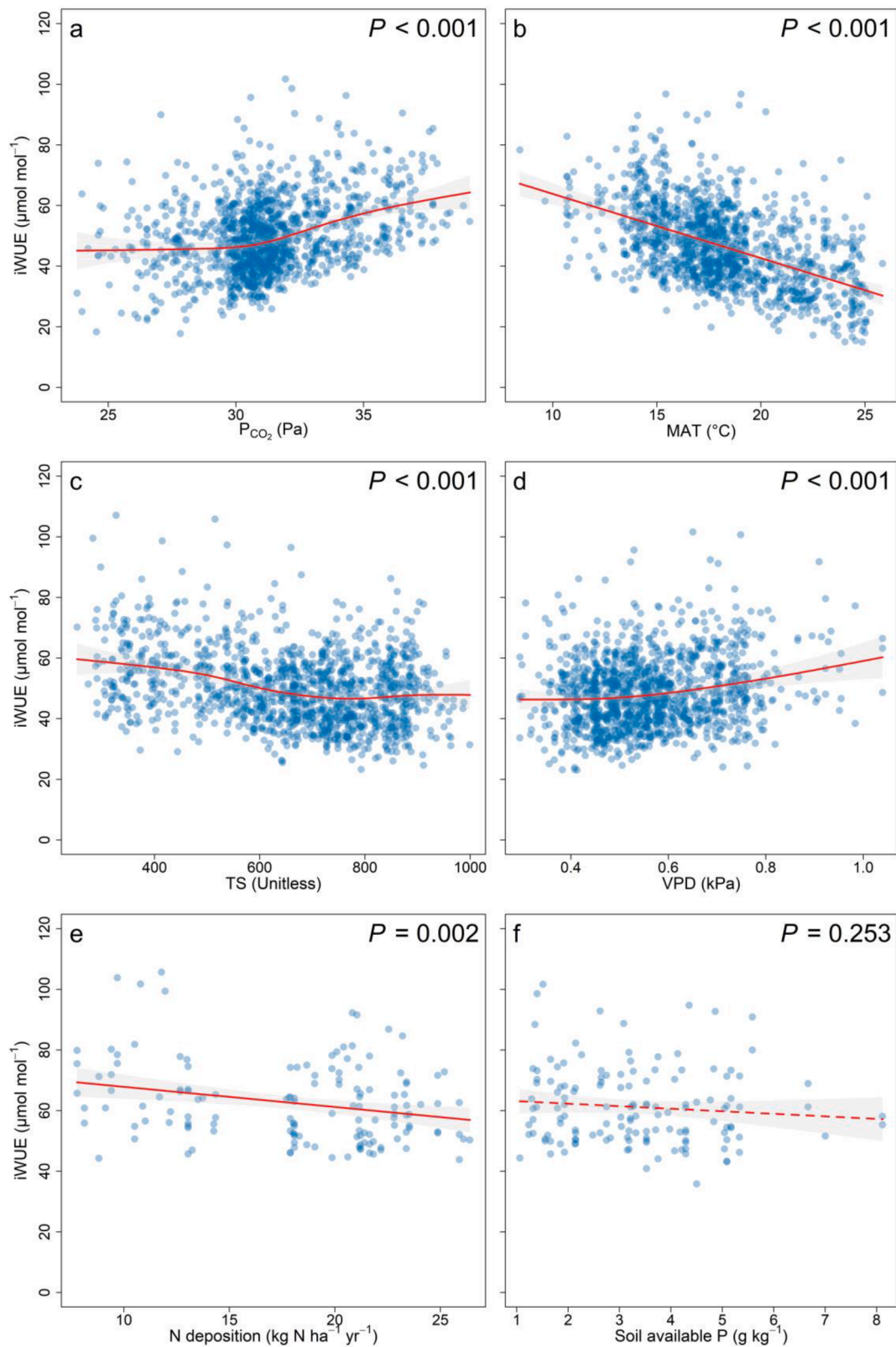
Fig. 4. Partial effects of partial pressure of CO_2 (a, P_{CO_2}), mean annual temperature (b, MAT), temperature seasonality (c, TS), vapor pressure deficit (d, VPD), N deposition (e), and soil available phosphorus concentration (soil available P, f) on iWUE. Blue dots represent partial residuals from the generalized additive mixed models (GAMMs), that is, the estimates for the variable plus the residuals. Red lines and gray shadings are, respectively, the predicted values and 95% confidence intervals from the GAMMs. Solid and dashed lines indicate fitted significant and non-significant results, respectively, at $P < 0.05$.

VPD can result in a decline in stomatal conductance, thus increasing iWUE (Grossiord et al., 2020). In contrast, high climatic variability might negatively affect iWUE by decreasing plant productivity (Newberry, 2010). The difference between our study and Huang et al. (2016) might be explained by the different time-scale (continuous vs discrete with large gaps) and region-scale (whole southern China vs several sites (Guling)). The discrete-time with large gaps and single sites might be affected by environmental events, e.g., temperature fluctuation and N deposition which can be avoided by using continuous-time and large-scale data sets. Specifically, the decreases of iWUE in Huang et al. (2016) were caused by huge differences in N deposition between 1950s and 2014 in Guling, with a negative correlation between N deposition and iWUE which was also observed in the present study and others (Lu et al., 2018). Although N deposition increased significantly, the increased rate significantly varied among sites in southern China (Yu et al., 2019). Furthermore, iWUE can also be affected by other environmental factors, i.e. CO_2, MAT, and VPD. Therefore, iWUE might increase on a larger studied scale, i.e. southern China, with decreases in special small sites such as Guling, where N deposition strongly increased over the past decades (Huang et al., 2016).

The patterns of annual rate of change of iWUE support another part of our first hypothesis that the strength of that response varies predictably across regions depending on climatic conditions, which might be caused by the diminishing effects of atmospheric CO_2 on iWUE (Adams et al., 2020) and the increases in air temperature and N deposition. There are several possible causes explaining the decline in annual rate of change of iWUE. First, although iWUE can increase at elevated atmospheric $[CO_2]$ as mentioned above, the increasing rate of change of iWUE may be constrained by increasing nutrient limitation (e.g., P) across biomes (Correa-Díaz et al., 2020; Liles et al., 2019; Maxwell and Silva, 2020; Peñuelas et al., 2017; Quadri et al., 2021; Wang et al., 2020b). Specifically, as the studied samples came from southeast China with sub-tropical/tropical mesic/wet and hot (on average) climates, the soils tend to be low in plant-available P (Hou et al., 2020). This, together with the increasing soil N saturation by continuous N deposition (Lu et al., 2018) should drive steadily increasing P limitation, which, in turn, can limit an increase in iWUE resulting from an increasing atmospheric CO_2 concentration (Adams et al., 2020). Second, high temperatures might increase water loss through transpiration and decrease iWUE (Matthews and Lawson, 2019). The MAT in southern China significantly increased since 1980 (Fig. S10b) which might limit the increases in plant iWUE and thus decreasing ΔiWUE. Third, the positive effects of N deposition on transpiration rates might also directly contribute to decreases in ΔiWUE. A 10-year experiment adding N to an already N-rich tropical forest in southern China showed that trees maintain foliar nutrient concentrations, which we also observed in the present study (Fig. S11), possibly due at least in part to increasing transpiration rates, and to iWUE generally decreasing with adding N (Lu et al., 2018). Fourth, high S deposition can compromise the formation of leaf cuticular waxes and stomatal structure due to altering the apoplastic pH and electrochemical potential gradient across the guard cell plasmalemma (Eamus and Fowler, 1990; Shepherd and Griffiths, 2006). Therefore, the high level of sulfur (S) deposition in China in the recent past (Yu et al., 2017; Zhao et al., 2021) can also cause a decline ΔiWUE via declining plant growth and productivity (Silva et al., 2015). Therefore, we surmise that the temporal patterns of the annual rate of change of iWUE in this study was most likely caused by increasingly severe P limitation and decreases in transpiration under high N deposition, high S deposition, global warming and continuously increasing atmospheric CO_2 concentrations (Adams et al., 2020; Hou et al., 2020; Yu et al., 2019).

The iWUE substantially declined from the west to the east of southern China, with higher values concentrated in the southwest (Fig. 2), partly coinciding with our second hypothesis and the findings of Li et al. (2019), and supporting Cooley et al. (2022) who found a remarkably variation in WUE even at a small spatial scale. The spatial pattern of iWUE in our study was consistent with the spatial patterns of

TS, VPD, and N deposition (Fig. S12), which suggests the important role of the three factors in impacting spatial patterns of plant iWUE in south China. It is worth mentioning that we did not observe significant correlations between plant iWUE and soil properties which might be attributed to the lack of long-term soil data. However, given the higher variation of soil properties in space than in time (Poggio et al., 2021) and the significant correlations between soil properties (e.g., soil pH, silt and clay) and foliar $\delta^{13}C$ or iWUE reported in previous studies (Cornwell et al., 2018; Maxwell et al., 2018), further studies should be conducted to address the role of soil properties affecting spatial patterns of iWUE in tropical and subtropical forests.

5. Conclusion

Mean iWUE of 12 common woody species increased by 15.7 μmol mol^{-1} over the past 90 years in southern China, but the annual rate of change in iWUE showed an S-curve pattern. We identified that temporal and spatial patterns of iWUE were associated with changes in atmospheric $[CO_2]$ (+), VPD (+), MAT (-), TS (-), and N deposition (-). Changes in $[CO_2]$, MAT, TS, VPD, and N deposition affected the temporal patterns, and changes in TS, VPD and N deposition impacted the spatial patterns. The present regional-scale patterns of iWUE of forest tree species help to improve predictions of ecological processes and functions including C and water cycles of forest ecosystems under global change.

Declaration of Competing Interest

The authors declare that they have no known competing financial interests or personal relationships that could have appeared to influence the work reported in this paper.

Acknowledgements

Supplementary materials

Supplementary material associated with this article can be found, in the online version, at doi:10.1016/j.agrformet.2022.109056.

References

Adams, M.A., Buckley, T.N., Turnbull, T.L., 2020. Diminishing CO_2 driven gains in water-use efficiency of global forests. Nat. Clim. Chang. 10 (5), 466–471.

Allan, R., Pereira, L., Smith, M., 1998. Crop evapotranspiration-Guidelines for computing crop water requirements-FAO Irrigation and drainage paper, 56. FAO-Food and Agriculture Organization of the United Nations, Rome, Italy.

Azen, R., Budescu, D.V., 2003. The dominance analysis approach for comparing predictors in multiple regression. Psychol. Methods 8 (2), 129–148.

Bernacchi, C.J., Singsaas, E.L., Pimentel, C., Portis, A.R., Long, S.P., 2001. Improved temperature response functions for models of Rubisco-limited photosynthesis. Plant Cell Environ 24 (2), 253–259.

Calcagno, V., de Mazancourt, C., 2010. glmulti: An R package for easy automated model selection with (generalized) linear models. J. Stat. Softw. 34 (12), 1–29.

Cerling, T.E., et al., 1997. Global vegetation change through the Miocene/Pliocene boundary. Nature 389 (6647), 153–158.

Cernusak, L.A., et al., 2019. Robust response of terrestrial plants to rising CO_2. Trends Plant Sci 24 (7), 578–586.

Cooley, S.S., Fisher, J.B., Goldsmith, G.R., 2022. Convergence in water use efficiency within plant functional types across contrasting climates. Nat. Plants 8 (4), 341–345.

Cornwell, W.K., et al., 2018. Climate and soils together regulate photosynthetic carbon isotope discrimination within C_3 plants worldwide. Glob. Ecol. Biogeogr. 27 (9), 1056–1067.

Correa-Díaz, A., et al., 2020. From trees to ecosystems: Spatiotemporal scaling of climatic impacts on montane landscapes using dendrochronological, isotopic, and remotely sensed data. Global Biogeochem. Cycles 34 (3), e2019GB006325.

Crawley, M.J., 2012. Mixed-Effects Models. In: Crawley, M.J. (Ed.), The R Book. John Wiley & Sons, Ltd, West Sussex, England, pp. 681–714.

Du, E., et al., 2020. Global patterns of terrestrial nitrogen and phosphorus limitation. Nat. Geosci. 13 (3), 221–226.

Eamus, D., Fowler, D., 1990. Photosynthetic and stomatal conductance responses to acid mist of red spruce seedlings. Plant Cell Environ 13 (4), 349–357.

Ehleringer, J.R., Cerling, T.E., 1995. Atmospheric CO_2 and the ratio of intercellular to ambient CO_2 concentrations in plants. Tree Physiol 15 (2), 105–111.

Farquhar, G.D., O'Leary, M.H., Berry, J.A., 1982. On the relationship between carbon isotope discrimination and the inter-cellular carbon-dioxide concentration in leaves. Aust. J. Plant Physiol. 9 (2), 121–137.

Farquhar, G.D., Richards, R.A., 1984. Isotopic composition of plant carbon correlates with water-use efficiency of wheat genotypes. Aust. J. Plant Physiol. 11 (6), 539–552.

Fick, S.E., Hijmans, R.J., 2017. WorldClim 2: new 1-km spatial resolution climate surfaces for global land areas. Int. J. Climatol. 37 (12), 4302–4315.

Giguere-Croteau, C., et al., 2019. North America's oldest boreal trees are more efficient water users due to increased CO_2, but do not grow faster. Proc. Natl. Acad. Sci. U.S.A. 116 (7), 2749–2754.

Graven, H., et al., 2017. Compiled records of carbon isotopes in atmospheric CO_2 for historical simulations in CMIP6. Geosci. Model. Dev. 10 (12), 4405–4417.

Grossiord, C., et al., 2020. Plant responses to rising vapor pressure deficit. New Phytol 226 (6), 1550–1566.

Harris, I., Osborn, T.J., Jones, P., Lister, D., 2020. Version 4 of the CRU TS monthly high-resolution gridded multivariate climate dataset. Sci. Data 7 (1), 109.

Hengl, T., et al., 2017. SoilGrids250m: Global gridded soil information based on machine learning. Plos One 12 (2), e0169748.

Hou, E., et al., 2020. Global meta-analysis shows pervasive phosphorus limitation of aboveground plant production in natural terrestrial ecosystems. Nat. Commun. 11 (1), 637.

Huang, R., et al., 2017. Does increasing intrinsic water use efficiency (iWUE) stimulate tree growth at natural alpine timberline on the southeastern Tibetan Plateau? Glob. Planet. Change 148, 217–226.

Huang, Z., et al., 2016. Long-term nitrogen deposition linked to reduced water use efficiency in forests with low phosphorus availability. New Phytol 210 (2), 431–442.

Jia, Y., et al., 2019. A spatial and temporal dataset of atmospheric inorganic nitrogen wet deposition in China (1996 - 2015). China Sci. Data 4 (1), 1–10.

Lanigan, G.J., Betson, N., Griffiths, H., Seibt, U., 2008. Carbon isotope fractionation during photorespiration and carboxylation in senecio. Plant Physiol 148 (4), 2013–2020.

Lenth, R.V., 2016. Least-squares means: The R package lsmeans. J. Stat. Softw. 69 (1), 1–33.

Li, X., Farooqi, T.J.A., Jiang, C., Liu, S., Sun, O.J., 2019. Spatiotemporal variations in productivity and water use efficiency across a temperate forest landscape of Northeast China. For. Ecosyst. 6, 22.

Liles, G.C., Maxwell, T.M., Silva, L.C.R., Zhang, J.W., Horwath, W.R., 2019. Two decades of experimental manipulation reveal potential for enhanced biomass accumulation and water use efficiency in ponderosa pine plantations across climate gradients. J. Geophys.Res-Biogeo. 124 (7), 2321–2334.

Liu, C., et al., 2018. Variation of stomatal traits from cold temperate to tropical forests and association with water use efficiency. Funct. Ecol. 32 (1), 20–28.

Liu, X., et al., 2013. Enhanced nitrogen deposition over China. Nature 494 (7438), 459–462.

Lu, X., et al., 2018. Plant acclimation to long-term high nitrogen deposition in an N-rich tropical forest. Proc. Natl. Acad. Sci. U.S.A. 115 (20), 5187–5192.

Marchand, W., et al., 2020. Strong overestimation of water-use efficiency responses to rising CO_2 in tree-ring studies. Glob. Chang. Biol. 26, 4538–4558.

Matthews, J., Lawson, T., 2019. Climate change and stomatal physiology. In: Roberts, J. (Ed.), Annual Plant Reviews. John Wiley & Sons, Ltd, West Sussex, England, pp. 1–39.

Maxwell, T.M., Silva, L.C.R., 2020. A state factor model for ecosystem carbon-water relations. Trends Plant Sci 25 (7), 652–660.

Maxwell, T.M., Silva, L.C.R., Horwath, W.R., 2018. Integrating effects of species composition and soil properties to predict shifts in montane forest carbon-water relations. Proc. Natl. Acad. Sci. U.S.A. 115 (18), E4219–E4226.

McCarroll, D., et al., 2009. Correction of tree ring stable carbon isotope chronologies for changes in the carbon dioxide content of the atmosphere. Geochim. Cosmochim. Acta 73 (6), 1539–1547.

McLauchlan, K.K., Ferguson, C.J., Wilson, I.E., Ocheltree, T.W., Craine, J.M., 2010. Thirteen decades of foliar isotopes indicate declining nitrogen availability in central North American grasslands. New Phytol 187 (4), 1135–1145.

Newberry, T.L., 2010. Effect of climatic variability on $\delta^{13}C$ and tree-ring growth in piñon pine (*Pinus edulis*). Trees 24 (3), 551–559.

Peñuelas, J., Canadell, J.G., Ogaya, R., 2011. Increased water-use efficiency during the 20th century did not translate into enhanced tree growth. Glob. Ecol. Biogeogr. 20 (4), 597–608.

Peñuelas, J., et al., 2017. Shifting from a fertilization-dominated to a warming-dominated period. Nat. Ecol. Evol. 1 (10), 1438–1445.

Peres-Neto, P.R., Legendre, P., Dray, S., Borcard, D., 2006. Variation partitioning of species data matrices: Estimation and comparison of fractions. Ecology 87 (10), 2614–2625.

Poggio, L., et al., 2021. SoilGrids 2.0: producing soil information for the globe with quantified spatial uncertainty. Soil 7 (1), 217–240.

Quadri, P., Silva, L.C.R., Zavaleta, E.S., 2021. Climate-induced reversal of tree growth patterns at a tropical treeline. Sci. Adv. 7 (22), eabb7572.

R Core Team, 2020. R: A language and environment for statistical computing. R Foundation for Statistical Computing, Vienna, Austria.

Shangguan, W., et al., 2013. A China data set of soil properties for land surface modeling. J. Adv. Model. Earth Syst. 5 (2), 212–224.

Sheffield, J., Goteti, G., Wood, E.F., 2006. Development of a 50-year high-resolution global dataset of meteorological forcings for land surface modeling. J. Clim. 19 (13), 3088–3111.

Shepherd, T., Griffiths, D.W., 2006. The effects of stress on plant cuticular waxes. New Phytol 171 (3), 469–499.

Silva, L.C.R., Gomez-Guerrero, A., Doane, T.A., Horwath, W.R., 2015. Isotopic and nutritional evidence for species- and site-specific responses to N deposition and elevated CO_2 in temperate forests. J. Geophys.Res-Biogeo. 120 (6), 1110–1123.

Silva, L.C.R., Lambers, H., 2021. Soil-plant-atmosphere interactions: structure, function, and predictive scaling for climate change mitigation. Plant Soil 461 (1-2), 5–27.

Silva, L.C.R., et al., 2016. Tree growth acceleration and expansion of alpine forests: The synergistic effect of atmospheric and edaphic change. Sci. Adv. 2 (8), e1501302.

Soh, W.K., et al., 2019. Rising CO_2 drives divergence in water use efficiency of evergreen and deciduous plants. Sci. Adv. 5 (12), eaax7906.

Stocker, B.D., et al., 2020. P-model v1.0: an optimality -based light use efficiency model for simulating ecosystem gross primary production. Geosci. Model. Dev. 13 (3), 1545–1581.

Tang, S., et al., 2022. Multiple environmental factors regulate the large-scale patterns of plant water use efficiency and nitrogen availability across China's forests. Environ. Res. Lett. 16, 034026.

Terrer, C., Vicca, S., Hungate, B.A., Phillips, R.P., Prentice, I.C., 2016. Mycorrhizal association as a primary control of the CO_2 fertilization effect. Science 353 (6294), 72–74.

Vogado, N.O., Winter, K., Ubierna, N., Farquhar, G.D., Cernusak, L.A., 2020. Directional change in leaf dry matter $\delta^{13}C$ during leaf development is widespread in C_3 plants. Ann. Bot. 126 (6), 981–990.

Wang, J., et al., 2020a. Large Chinese land carbon sink estimated from atmospheric carbon dioxide data. Nature 586 (7831), 720–723.

Wang, S., et al., 2020b. Recent global decline of CO_2 fertilization effects on vegetation photosynthesis. Science 370 (6522), 1295–1300.

Yu, G., et al., 2019. Stabilization of atmospheric nitrogen deposition in China over the past decade. Nat. Geosci. 12 (6), 424–429.

Yu, H., et al., 2017. Development of atmospheric acid deposition in China from the 1990s to the 2010s. Environ. Pollut. 231, 182–190.

Zhao, W., Zhao, Y., Ma, M., Chang, M., Duan, L., 2021. Long-term variability in base cation, sulfur and nitrogen deposition and critical load exceedance of terrestrial ecosystems in China. Environ. Pollut. 289, 117974.

Zhao, Y., et al., 2022. Decline in bulk deposition of air pollutants in China lags behind reductions in emissions. Nat. Geosci. 15 (3), 190–195.